A Computational Study of the Interaction of C_2 Hydrocarbons with CuBTC

Rui Afonso[1], Jordi Toda[1], José R. B. Gomes[1,*], Michael Fischer[2,3], Christopher Campbell[4], Miguel Jorge[4]

[1] CICECO – Center for Research in Ceramics and Composite Materials, Department of Chemistry,University of Aveiro, Campus Universitário de Santiago, 3810-193 Aveiro, Portugal

[2] Crystallography Group, Department of Geosciences, University of Bremen, Klagenfurter Straße 2-4, 28359 Bremen, Germany

[3] MAPEX Center for Materials and Processes, University of Bremen, Bibliotheksstraße 1, 28359 Bremen, Germany

[4] Department of Chemical and Process Engineering, University of Strathclyde, 75 Montrose Street, GlasgowG1 1XJ, United Kingdom

* Corresponding Author. E-mail: jrgomes@ua.pt. Phone: +351 234 401 423. Fax: +351 234 401 470

Abstract:

The adsorptions of ethane, ethene, and ethyne over the coordinatively unsaturated sites (CUS) of copper (II) benzene-1,3,5-tricarboxylate (CuBTC) were studied by means of density functional theory (DFT), using both cluster or periodic models. Exchange-correlation functionals from different rungs of the Jacobs ladder of the DFT were used and energies were corrected for the basis superposition error either through extrapolation to the complete basis set limit or upon the consideration of the Counterpoise method. From the calculated data, it was found that the adsorbate to CUS distances decrease in the order ethane > ethene ≈ ethyne and that the strength of adsorption increase in the order ethane to ethyne to ethene. The energies of interactions of ethene and ethyne with the CUS of CuBTC are approximately the double of that calculated for ethane. The calculated adsorption energies and geometries are in very satisfactory agreement with the available experimental results. The results of topological analyses confirm that the unsaturated bonds of ethene and ethyne form open shell like bonds with the CUS while interaction with ethane have predominant closed shell character.

Keywords: HKUST-1; Adsorption; Separation; Density Functional Theory; Cluster Models; Periodic Models; Copper Paddlewheel.

1. Introduction

The separation of mixtures of light alkanes and alkenes, such as ethane and ethene (a.k.a. ethylene), is an important problem in the chemical industry [1, 2]. Currently, this separation is typically achieved by cryogenic distillation [1, 2]. This is a very energy-intensive process, which has fomented the search for alternatives. The selective removal of acetylene is another problem of interest, as it may accumulate in low-temperature plants, *e.g.* air separation units, causing the risk of violent decomposition [3]. Adsorption-based techniques have been proposed as promising energy-efficient technologies for the selective separation of alkenes or alkynes [4-6]. These processes are based on the preferential adsorption of one component over the other in a solid adsorbent. Different criteria, such as the working capacity, the adsorption selectivity, and the regenerability, determine the suitability of the adsorbent. For alkane/alkene separations, π-complexing sorbents have shown high selectivities. In these systems, the alkene strongly interacts with a cation site, such as Cu^+ or Ag^+, through orbital interactions. This leads to a strongly preferred adsorption of the alkene over the alkane. Cation-impregnated amorphous silica materials [7, 8] and mesoporous silicas [9, 10] as well as zeolites [11, 12] have been investigated in this context.

Metal-organic frameworks (MOFs) are crystalline hybrid materials that have attracted considerable scientific interest in the last 20 years. Because these materials often exhibit high porosities, as well as the possibility to incorporate functional groups or accessible metal sites in the pore wall, they are widely regarded as promising new adsorbent materials for separation applications [13-16]. The properties of various MOFs have been investigated in terms of their performance for alkane/alkene separation, and acetylene removal [17-20]. Most focus has been placed on MOFs with coordinatively unsaturated sites (CUS), where it can be expected that the unsaturated hydrocarbons will preferentially adsorb at the metal centers due to significant metal-π-interactions [21-23]. For example, the M-MOF-74 series (with M = Mg, Mn, Fe, Co), containing open metal sites (OMS), has been studied for alkane/alkene separation, and particularly high selectivities for C_2 and C_3 alkenes over the corresponding alkanes were observed for Co-MOF-74 [24, 25], and Fe-MOF-74 [22, 26]. Co-MOF-74 also exhibits a very high acetylene uptake capacity [27]. Cu-BTC (also known as MOF-199 or HKUST-1) exhibits preferential adsorption of propylene over propane, with a C_3H_6/C_3H_8 selectivity of about 3 [28-31], at low pressures. The same system selectively adsorbs isobutene over isobutene [32], and shows an exceptionally high acetylene uptake at room temperature, rendering it interesting for acetylene storage and, possibly, selective C_2H_2 adsorption [33-35]. Other MOFs with open

copper sites in a Cu dimer paddlewheel, like the one possessed by CuBTC (Figure 1), exhibit similar alkane, alkene and alkyne adsorption properties [19, 34-38].

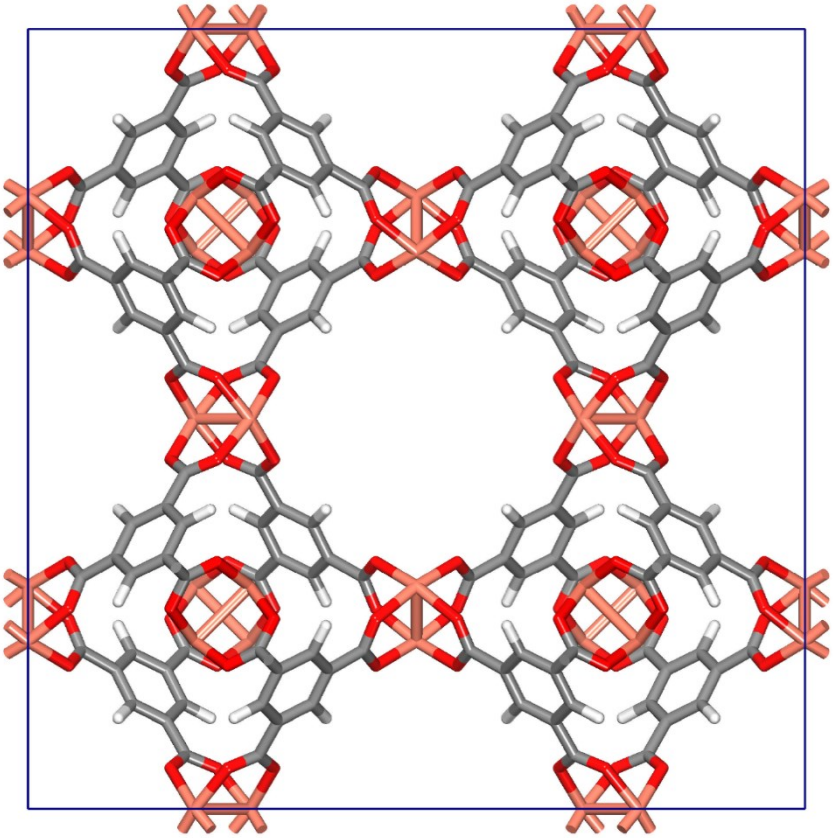

Figure 1. The periodic structure of activated CuBTC (i.e. after solvent removal, leaving unsaturated metal sites). Color code: Orange is copper; red is oxygen; grey is carbon; and white is hydrogen.

Most computational studies of adsorption in MOFs rely on grand-canonical Monte Carlo simulations using empirical force fields [39, 40]. However, it has been shown that standard force-fields are incapable of describing the localized interaction of molecules such as hydrogen, methane, acetylene, or ethylene with CUS-containing materials [28, 39-44]. There are different strategies to overcome this limitation [44-46]. A pragmatic approach is the derivation of improved parameter sets from density-functional theory (DFT) calculations of adsorption energies at the CUS [41-44, 47-49]. This strategy has yielded good results for alkanes, alkenes and alkynes in CUS-containing MOFs [19, 43, 44, 50-54].

In addition to the issue of parameter derivation for simulations of macroscopic properties, first-principles investigations of the interaction of adsorbed molecules with accessible metal sites are important to gain more fundamental insights into the nature of the metal-guest interaction. Several DFT approaches have been used to model the interaction of different adsorbate

molecules with accessible copper sites in the CuBTC paddlewheel [51, 53, 55-59]. Typically, periodic models with the Vienna ab-initio Simulation Package (VASP) are used, with plane-wave basis sets and projected augmented-wave (PAW) pseudo-potentials and a dispersion correction-containing functional, like PBE-D3 [57, 59] or vdW-DF2 [53, 56]. In general, good agreement of the calculated interaction enthalpies with available experimental heats of adsorption has been observed, indicating that this is a successful approach to simulate MOFs with open copper sites. Despite the encouraging results, the experimental information regarding the structures of adsorbed ethane, ethene and ethyne (a.k.a. acetylene) is scarce [33]. Moreover, the experimental isosteric heats of adsorption may differ by up to 10 $kJ \cdot mol^{-1}$ [51, 53, 55-59]. Previously, we have performed a careful computational study on the comparison of several different DFT exchange-correlation functionals on the interaction of water with a Cu dimer paddlewheel representative of the inorganic nodes of CuBTC [60]. It was found that B2PLYP-D, a double-hybrid functional with dispersion corrections, and Minnesota functionals based on the meta-generalized gradient approximation (meta-GGA), like the local M06-L functional, were well-suited for geometry optimization and for calculating the enthalpy of adsorption of water molecules interacting with the CUS of CuBTC.

Based on the excellent behavior of such methods, we are now presenting a detailed theoretical study of the adsorption process of C_2H_6, C_2H_4 and C_2H_2 over CuBTC [61, 62]. The calculations considered the computationally expensive but highly accurate B2PLYP-D, the optimal compromise solution M06-L, and the cheap, but predictably less accurate [63], PBE. For comparison of the effects introduced by the consideration of the crystalline structure of CuBTC, we have also performed calculations where a unit cell of CuBTC is periodically repeated in three dimensions. Since the B2PLYP-D functional was not available in the computer code used to run the periodic calculations, another dispersion corrected functional was used, PBE-D3, which was also found to be quite accurate in modelling interaction with CUSs [63]. To the best of our knowledge, B2PLYP-D and M06-L have never been used to model these systems. The adsorption mechanism was also deeply investigated through detailed topological analyses.

2. Computational details

Spin polarized DFT calculations within a periodic model approach were performed with the CP2K code [64], employing the Perdew-Burke-Ernzerhof (PBE) exchange-correlation functional [65, 66] (without and with D3 dispersion corrections [67]) and with the Minnesota 2006 local functional (M06L)[68]. The periodic structure of CuBTC (Figure 1) was modeled with a rhombohedral primitive cell (not shown) containing 156 atoms, with the length of the *a*, *b* and *c* vectors equal to the experimental value, i.e., 18.6273 Å. The basis sets used were double-ζ plus polarization (DZVP) with PBE-optimized Goedecker-Teter-Hutter (GTH) pseudopotentials [69, 70] for all the atoms in PBE and PBE-D3 calculations, employing an energy cutoff of 600 Ry. For obtaining converged structures in the case of the M06-L calculations, the energy cutoff was increased to 800 Ry, using a double-ζ plus polarization (DZVP) basis set for Cu and triple-ζ plus polarization (TZVP) basis sets for the remaining atoms together with GTH potentials. Furthermore, a single point counterpoise correction [71] was used to account for basis set superposition error (BSSE).

Cluster model calculations were also performed using a reduced model of the CuBTC framework, the copper formate ($Cu_2(COOH)_4$) cluster, where the benzene groups have been replaced by terminal hydrogens (Figure 2). Some calculations were also performed with a copper benzoate ($Cu_2(COOC_6H_5)_4$) model for comparison purposes (see below). This small model reliably reproduces the local environment of the copper atoms in the extended framework, allowing us to test our functionals while significantly reducing the computational cost [42, 44, 60]. The calculations with the cluster model approach were carried out using the Gaussian 09 code [72]. Three density functionals were used: B2PLYP-D, a double-hybrid functional with empirical long-range dispersion corrections [73, 74], M06-L, and PBE. Single-point calculations considering the CCSD(T) approach [75] were also performed for comparison purposes. All the structures including the CuBTC paddlewheel have been calculated considering a triplet electronic state. Isolated adsorbate molecules were calculated considering a singlet electronic state. Correlation-consistent valence X-ζ basis sets with polarization functions by Dunning et al. were used for O, C and H, namely cc-pVDZ [76] and cc-PVTZ [77] basis sets, while the pseudopotential-based correlation consistent basis sets (cc-pVDZ-PP or cc-pVTZ-PP) by Peterson et. al. [78, 79] were employed for Cu. The complete basis set (CBS) energy (and enthalpy) limit was obtained by two-points extrapolation of the cc-pVDZ and cc-pVTZ energies (and enthalpies) using the Truhlar's scheme [80]. This choice is justified by the

computational hurdle associated with calculations using quadruple-ζ basis sets correlation consistent basis sets, with a detailed discussion about this extrapolation procedure being presented in the Supporting Information. A previous study [41] showed that adsorption of a single adsorbate molecule over the open metal sites of a CuBTC cluster causes distortion of the structure, whereby the two copper atoms move towards the adsorbate. This is unrealistic, as such behavior does not take place in the periodic model or in the real material. In order to retain the symmetry of the paddlewheel, two molecules have been adsorbed simultaneously on each Cu atom of the cluster. Interaction energies were calculated using the formula,

$$E_{interaction} = \frac{E_{complex} - E_{CuBTC} - 2\,E_{adsorbate}}{2} \quad (1)$$

where $E_{interaction}$ is the interaction energy, $E_{complex}$ is the energy of the CuBTC paddlewheel interacting with two adsorbate molecules, E_{CuBTC} is the energy of the isolated CuBTC paddlewheel and $E_{adsorbate}$ is the energy of a single isolated adsorbate molecule. An analogous formula was used for enthalpy calculations. Topological analysis of the optimized clusters was performed using the Multiwfn 3.6 code [81].

3. Results and discussion

In this section, we analyze the possible orientations of the adsorbates at the vicinity of the CUS as obtained with the different computational strategies (Section 3.1). Then, in Section 3.2, we discuss the most important geometrical aspects from the computations, namely, the Cu-Cu and the Cu-C distances. Section 3.3 compares the calculated adsorption energies and enthalpies of the different levels of theory with available experimental isosteric heats of adsorption. Finally, in Section 3.4, we perform a detailed topological analysis of the adsorbate to substrate binding.

3.1. Local adsorbate orientations

For cluster DFT calculations, it was possible to successfully optimize all clusters. For M06-L and PBE, vibrational frequencies were determined, making it possible to assess whether a certain optimized geometry was a true minimum. It was always possible to find at least one energy minimum for each cluster. Due to computational limitations, frequencies were not determined with B2PLYP-D. Examples of optimized clusters are shown in Figure 2 for B2PLYP-D/cc-pVTZ, in principle the highest level of theory employed here. Similar figures for the PBE and M06-L functionals are provided in the Supporting Information (Figures S1 and S2). It is immediately apparent that ethene and ethyne (i.e. acetylene) adopt a centered configuration, due to the strong interaction between the open copper site and the π orbitals of the unsaturated C-C bonds. On the other hand, ethane is shifted, with the interaction with the open copper sites being mainly through the -CH_3 terminations. Shifted structures from DFT calculations were reported in the literature for ethane interacting with cluster models for the CUS of Cu-TDPAT, [82] and of Fe-MOF-74. [22]

The optimization procedures of the cluster calculations have resulted in minima (or saddle points) in two distinct molecular configurations; with the C-C axis of the adsorbate molecule parallel to one of the O-C-O axes of the paddlewheel, or midway between the two O-C-O axes. We have named these geometric configurations as “in-line” and “in-between”, respectively. Examples of the two can be seen in Figures 2 and 3. These two geometric configurations are usually energetically similar, with differences of just a few kJ/mol between the two (Table 1), indicating that both are probably present in the real system. It was always possible (though not always easy) to obtain the in-line configuration, for all adsorbates, models and basis sets. However, there were a few cases where it proved impossible, despite our best efforts, to obtain the in-between configuration. The latter case is represented with a dash in Table 1.

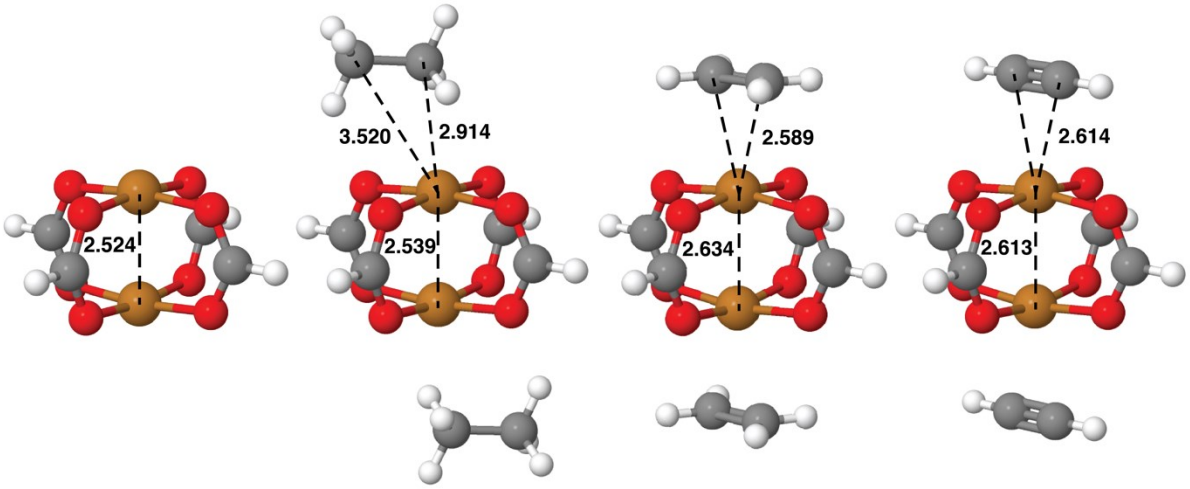

Figure 2. Cu-formate paddlewheel geometry, as modelled with B2PLYP-D and cc-pVTZ. From left to right are representations of the bare paddle wheel, with adsorbed ethane (in-between), with adsorbed ethene (in-line) and with adsorbed ethyne (in-line).Numbers indicate distances in Å.

Table 1. Energy difference, in kJ/mol, between in-line and in-between geometric configurations for adsorbate molecules interacting with the Cu-formate cluster model. Negative values indicate that in-line configuration is the most stable. Horizontal dashes indicate cases where it was not possible to obtain optimized in-between molecular configurations.

	Ethane		Ethene		Ethyne	
	cc-pVDZ	cc-pVTZ	cc-pVDZ	cc-pVTZ	cc-pVDZ	cc-pVTZ
PBE	—	—	+2.3	-0.2	—	—
M06-L	+4.1	+4.6	-2.0	-5.4	-1.1	-0.1
B2PLYP-D	-0.7	+1.5	+0.7	-0.7	—	—

Top views of the most stable clusters obtained for ethene are shown in Figure 3. Equivalent images for ethane and ethyne are shown in Figures S4 and S5. The difference between the two geometric configurations is made clear in these Figures. The in-line geometric configuration is preferred in all cases for ethyne. For ethane and ethene, the situation is more balanced, with a similar number of cases where each of the configurations is preferred. The three cases, for PBE and M06-L, where the in-between configuration is more favorable correspond to situations where the in-line optimizations yielded meta-stable (saddle points) geometries, with imaginary frequencies. The reverse is not true; only in one case (ethene, M06-L, cc-pVDZ) does the in-between configuration correspond to a meta-stable geometry. Interestingly, for ethyne, all optimizations yielded in-line true energy minima, probably a reflection of the simpler system, with a reduced number of atoms.

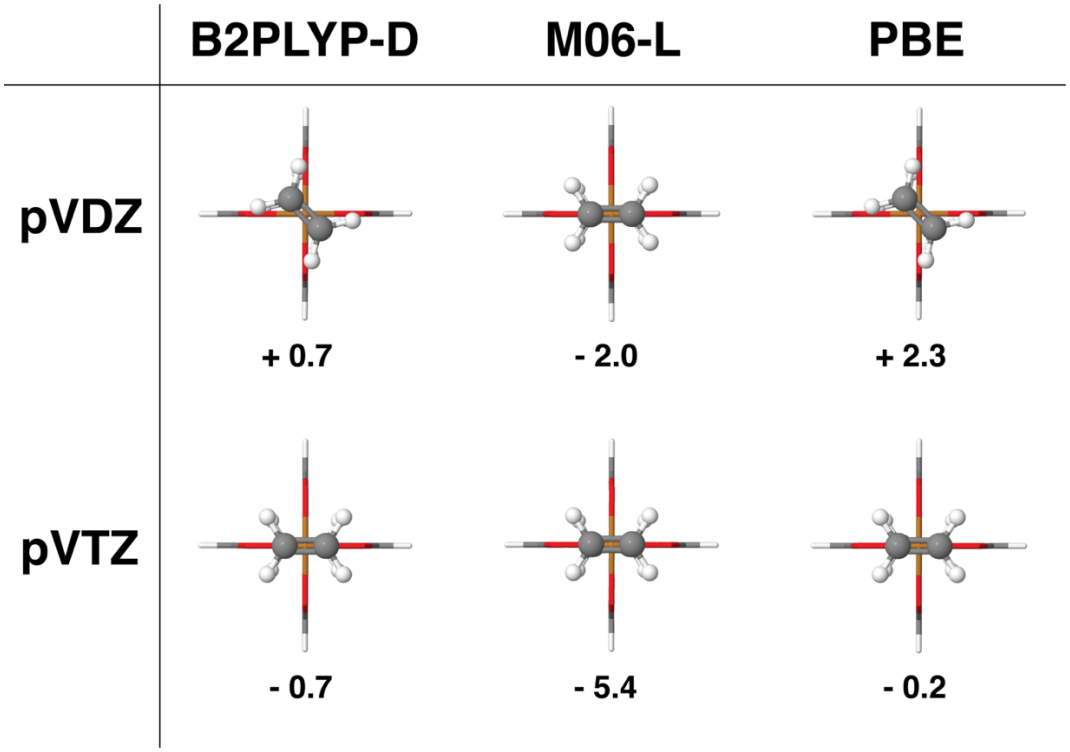

Figure 3. Upper view of the most stable geometric configuration of ethene in CuBTC, for different theoretical models and basis sets. Energy differences (kJ/mol) between in-line (negative values) and in-between (positive values) configurations, taken from Table 1, are shown below each cluster image.

For periodic calculations, all optimizations yielded an in-between geometry. This marked difference when compared to cluster calculations is probably due to the use of a too simple model in the latter. To confirm this hypothesis, we have performed M06-L calculations for the ethyne interaction with the larger copper benzoate ($Cu_2(COOC_6H_5)_4$) cluster. While the M06-L calculations with the copper formate ($Cu_2(COOH)_4$) cluster are in favor of the in-line geometry, it was not possible to find any stable in-line structure (i.e. without imaginary frequencies) when using the larger benzoate model, with all calculations yielding the in-between adsorption mode (Figure S3). We calculated the natural atomic charges (Table S3) for the large and small clusters interacting with the ethyne molecule (constraints were used to impose an in-line geometry in the benzoate model). Since the natural atomic charges (q) of the ethyne's constituting atoms are practically the same in the four systems (two geometries, two cluster models, with $\Delta q < 0.01$ e), it is suggested that the preference for the in-between adsorption mode in the periodic calculations is a consequence of the next-nearest neighbor interactions of the atoms of the adsorbate molecules with the aromatic moieties.

3.2. Comparative analysis of calculated geometries

For cluster calculations, the combination of three adsorbates, three functionals, two basis sets and two molecular geometric configurations corresponds to 36 optimizations. Plus the 6 sets of results for the free paddlewheel, gives a total of 42 optimizations. Detailed results of these 42 optimizations, taken from the Gaussian output files, are provided as Supplementary Information, except when redundant (the aforementioned cases where it was not possible to obtain a stable or meta-stable in-between configuration). For periodic calculations, three adsorbates plus the free paddlewheel and three basis sets gives a total of 12 optimizations. Atom coordinates of the final geometry of these optimizations are provided as Supplementary Information. For reference and comparative purposes, selected interatomic distances of optimized clusters of the bare paddlewheel and the three adsorbates with the cc-pVTZ basis set are shown in Table 2, while the parameters calculated with the cc-pVDZ basis set are shown in Table S1. The geometric parameters of periodic optimizations are shown in Table 3.

The experimental Cu-Cu distance of the bare paddlewheel is 2.50 ± 0.02 Å [62]. M06-L does the best job at describing this distance, both for cluster and periodic calculations, even though PBE-D3 and B2PLYP-D are also very close. In our previous work with H_2O as adsorbate [60], M06-L was clearly worse than B2PLYP-D in predicting both Cu-Cu and Cu-O_w distances, so it is somewhat surprising that they perform similarly in the case of the bare paddlewheel. As expected, PBE stands out from the others in giving estimates clearly outside (below) the experimental estimate range. Comparing the results from cluster and periodic calculations, the quality of the estimation is similar for both PBE and M06-L when the cc-pVTZ basis set is used in the cluster calculations, but cluster-based distances are underestimated when cc-pVDZ is employed. Thus, only the better (and much more computationally demanding) approach in the cluster calculations was able to replicate the level of accuracy of the periodic calculations.

Table 2. Distances of the optimized systems, from calculations with the PBE, M06-L and B2PLYP-D approaches and the cc-pVTZ basis set.[a] All values in Å.

Adsorbate	Approach	in-between				in-line			
		Cu-Cu	Cu-axis	Cu-C_1	Cu-C_2	Cu-Cu	Cu-axis	Cu-C_1	Cu-C_2
Ethane	PBE	—	—	—	—	2.485	3.462	3.069	3.965
	M06-L	2.511	3.092	2.788	3.535	2.515	3.219	2.808	3.739
	B2PLYP-D	2.539	3.140	2.914	3.520	2.541	3.222	2.941	3.644
Ethene	PBE	2.583	2.593	2.681	2.675	2.583	2.562	2.648	2.648
	M06-L	2.597	2.534	2.619	2.621	2.587	2.505	2.592	2.592
	B2PLYP-D	2.638	2.523	2.609	2.611	2.634	2.502	2.589	2.589
Ethyne	PBE	—	—	—	—	2.565	2.580	2.650	2.650
	M06-L	2.573	2.521	2.592	2.591	2.578	2.522	2.593	2.593
	B2PLYP-D	—	—	—	—	2.613	2.544	2.614	2.614

[a]Cu-Cu distances in the bare paddlewheel are 2.465 (PBE), 2.498 (M06-L) and 2.524 (B2PLYP-D).

Table 3. Distances, in Å, for structures obtained by periodic calculation optimizations.[a]

Adsorbate	Approach	Cu-Cu	Cu-axis	Cu-C_1	Cu-C_2
Ethane	PBE	2.502	3.546	3.076	4.105
	PBE-D3	2.503	3.247	3.009	3.633
	M06-L	2.509	3.243	3.005	3.627
Ethene	PBE	2.600	2.653	2.734	2.739
	PBE-D3	2.636	2.525	2.610	2.614
	M06-L	2.516	2.648	2.724	2.737
Ethyne	PBE	2.584	2.616	2.684	2.685
	PBE-D3	2.600	2.534	2.605	2.605
	M06-L	2.620	2.596	2.665	2.665

[a]Cu-Cu distances in the bare paddlewheel are 2.471 (PBE), 2.479 (PBE-D3) and 2.504 (M06-L).

To the best of our knowledge, there is only a single report mentioning experimental distances with which to compare the results of our calculations. Xiang et al. [33], using neutron powder diffraction, determined a Cu−C bonding distance of 2.62 Å for deuterated acetylene interacting with CuBTC. Based only on this result, in the cluster model calculations the best agreement is found for the B2PLYP-D approach, but the other approaches also performed satisfactorily. In the case of the periodic calculations, the best agreement is found for the PBE-D3 approach (Δ=0.015 Å) with slightly larger differences found for M06-L (Δ=0.045 Å) and PBE (Δ=0.064 Å).

Compared to previous DFT studies with MOFs possessing the Cu-dimer paddlewheel [82, 83], the Cu-C distances obtained in cluster calculations (Table 2) are slightly lower and those obtained in periodic calculations (Table 3) are slightly higher. One study, by Kulkarni and Sholl [51], reported a 2.8 Å Cu-axis distance for C_2H_2 calculated using the vdW-DF2 functional, a value higher than any of our estimates. Another study, by Zhang et al. [58], estimated a ~2.6 Å distance, also for C_2H_2, both with PBE and PBE-D2, a value in the same range as ours. Some of us reported also vdW-DF2 results, within a plane wave approach, for ethene adsorption in a periodic model of CuBTC[44]. The calculated bond distance between the midpoint of the C═C double bond and the copper atom was 2.648 Å, the C-Cu distance was 2.730 Å and the Cu-Cu distance was 2.716 Å. These values are larger than those obtained with the cluster model

calculations (Table 2). The periodic results from this work are much closer to the vdW-DF2 results [44].

Some interesting trends can be observed in the data provided in Tables 2 and 3. A uniform trend across both cluster and periodic calculations is that Cu-Cu distances increase, for all models, with the introduction of an adsorbate into the system. This has also been observed, both experimentally and computationally, in relation to H_2O [60, 62], and it stems mainly from the decrease in electronic density between the copper atoms, which leads to a slightly weaker interaction. Variation of Cu-Cu distances with the kind of adsorbate is also relatively uniform; there is a typical sequence ethane > ethyne > ethene, both for periodic and cluster calculations, perhaps functioning as a good proxy for paddlewheel-adsorbate interaction strength (see energetic analysis below). For Cu-C distances, the scenario is a bit more complex. Ethene and ethyne are, naturally, always closer to the copper atoms than ethane, but the relation between the two is more varied. For cluster calculations, Cu-C distances are larger for ethyne than ethene, with the exception of results for PBE/cc-PVDZ. For periodic calculations, PBE-D3 and M06-L also show the ethyne > ethene trend, with PBE again showing the reverse behavior. It seems that PBE with no dispersion correction is incapable of adequately describing the interaction of ethene and ethyne with the open copper sites. The energetic analysis below will further confirm this observation.

In cluster calculations, Cu-C distances increase from cc-pVDZ to cc-pVTZ. This trend is most pronounced for PBE calculations. It seems an increased number of electronic orbitals under consideration pushes the atoms slightly apart. The Dunning correlation consistent polarized valence basis sets [76, 77, 84] are reliably more accurate for larger shells of polarization functions. Taking a similar approach to that applied to total interaction energy extrapolation to complete basis set (see below), it can be tentatively asserted that cc-pVDZ distances are underestimated to a greater extent than those of cc-pVTZ, and, perhaps, cc-pVTZ distances would also be slightly underestimated relative to potential cc-pVQZ calculations.

In regards to variation of the exchange-correlation functional, there is also a clear pattern, both for periodic and cluster calculations. In cluster calculations, there is a systematic B2PLYP-D > M06-L > PBE trend for Cu-Cu distances, and PBE > B2PLYP-D > M06-L for Cu-C distances. For periodic calculations, with the exception of the ethene/M06-L data point, there is a clear M06-L > PBE-D3 > PBE trend in Cu-Cu distances. For Cu-C distances, the trend is PBE > M06-L > PBE-D3 for ethene and ethyne, and PBE > PBE-D3 > M06-L for ethane. In general, it is clear that the non-dispersion-corrected PBE is incapable of taking into full account

adsorbate-paddlewheel interactions, as expected [63], thus overestimating Cu-C distances, and underestimating Cu-Cu distances.

For cluster calculations, M06-L Cu-Cu distances are midway between those of PBE and B2PLYP-D for the bare paddlewheel and with ethane, but for ethene and ethyne, B2PLYP-D values become significantly larger than the other two. However, for Cu-C distances, M06-L and B2PLYP-D have very similar values (in particular for ethene and ethyne) when compared to PBE. Taking also into account the energetic results (Tables 4 and 5), it seems M06-L and B2PLYP-D provide a similar picture for the Cu-C_2H_x interactions, especially for ethene and ethyne adsorbates. Such a trend can also be observed for the Laplacian of energy density (Table 6), from the electronic topological analysis (see below).

For periodic calculations, application of dispersion-correction to PBE has a large effect on Cu-C distances, drawing the adsorbate molecule significantly closer to the paddlewheel, and closer even than with M06-L. Interestingly, Cu-Cu distances are barely affected for the bare cluster and ethane, and only mildly affected for ethene and ethyne; i.e., the dispersion correction influences mainly Cu-C distances. Periodic calculations with an in-between geometry generate PBE and M06-L values similar to those of in-between cluster calculations (Table S1), with no systematic deviation from one another.

3.3. Comparative analysis of calculated adsorption energies

Interaction energies, calculated using eq. (1), are shown in Table 4, for cluster calculations, and Table 6, for periodic calculations. Interaction enthalpies, for cluster calculations, are shown in Table 5. For cluster calculations, given that we have both cc-pVDZ and cc-pVTZ data, it was possible to perform an extrapolation to complete basis set. The two sets of extrapolated data refer to the basis set used to optimize the geometry. For example, when cc-pVDZ was used for optimization, the resulting geometry (either in-line or in-between) would then be used to perform a single-point calculation with cc-pVTZ. The two energies, referring to the same geometry, were then used to perform the extrapolation procedure. Enthalpies were determined, both for extrapolated and non-extrapolated values, by adding the relevant thermal corrections given through frequency determination. For B2PLYP-D, having not been possible to calculate frequencies, the thermal corrections of M06-L were added to its energy result, to yield pseudo-B2PLYP-D interaction enthalpies.

The first salient point in Tables 4 and 5 is that the interactions of ethene and ethyne are much more favorable than that of ethane. This observation holds true independently of the model, basis set or whether or not extrapolation was performed. Energies from periodic calculations in

Table 6 show the same trend. In both cases, even PBE is capable of adequately predicting that the π-metal interactions in ethyne and ethene are stronger than the general London interactions between ethane and the open copper sites. Still, as with distances in Table 2, interaction energies estimated using M06-L and B2PLYP-D in Table 4 are extremely close, and much more negative, than those estimated with PBE. As is discussed below regarding the interaction enthalpies of Table 5, M06-L results (and, therefore, also those of B2PLYP-D) are much more reliable than those of PBE. In fact, for calculations with the cc-pVDZ basis set, M06-L and B2PLYP-D energies are close to those obtained with the CCSD(T) approach (values in parenthesis in Table 4), but with the M06-L estimates being systematically slightly less negative than those of B2PLYP-D and slightly more negative than those of CCSD(T).

Table 4. Extrapolated and non-extrapolated interaction energies of ethane, ethene and ethyne with CuBTC, in kJ/mol, for cluster calculations.

Adsorbate	Approach	cc-pVDZ geometry		cc-pVTZ geometry	
		Extrapolated	Non-extrapolated	Extrapolated	Non-extrapolated
Ethane	PBE	-4.5	-12.5	-5.3	-7.0
	M06-L	-20.8	-24.4	-20.9	-21.7
	B2PLYP-D	-19.1	-24.9 (-20.4)[a]	-20.5	-21.5
Ethene	PBE	-21.9	-30.4	-22.4	-24.3
	M06-L	-42.5	-43.5	-43.1	-43.5
	B2PLYP-D	-40.7	-47.0 (-42.8)[a]	-41.2	-42.6
Ethyne	PBE	-20.9	-30.5	-21.2	-23.5
	M06-L	-38.8	-41.8	-38.6	-39.4
	B2PLYP-D	-35.1	-42.3 (-39.9)[a]	-35.2	-37.0

[a]CCSD(T) results obtained from single-point calculations using the B2PLYP-D geometry.

Comparing results from cluster calculations (cc-pVTZ extrapolated) and periodic calculations in Table 4 and Table 6, we can see that they are extremely close to each other for both PBE and M06-L, with periodic-based energies being slightly lower (i.e. more negative) by about 1-2 kJ/mol. This level of agreement, as observed also for inter-atomic distances, confirms that calculations using small clusters can be a good substitute for more computationally demanding periodic calculations. The results from separate cluster model calculations with the CCSD(T)/cc-pVDZ approach further support this inference (Table 4).

Table 5. Extrapolated and non-extrapolated interaction enthalpies of ethane, ethene and ethyne with CuBTC, at T = 298 K, in kJ/mol, for cluster calculations.

Adsorbate	Approach	cc-pVDZ geometry		cc-pVTZ geometry	
		Extrapolated	Non-extrapolated	Extrapolated	Non-extrapolated
Ethane	PBE	0.4	-7.5	-0.5	-2.2
	M06-L	-15.8	-19.5	-16.1	-17.0
	B2PLYP-D*	-14.1	-20.0	-15.7	-16.8
Ethene	PBE	-16.5	-25.0	-16.9	-18.8
	M06-L	-38.0	-38.9	-37.7	-38.1
	B2PLYP-D*	-36.1	-42.5	-35.9	-37.3
Ethyne	PBE	-17.4	-27.0	-17.5	-19.8
	M06-L	-34.6	-37.7	-35.2	-36.0
	B2PLYP-D*	-31.0	-38.2	-31.8	-33.5

* Enthalpic thermal corrections for B2PLYP-D results were taken from M06-L frequency calculations.

Table 6. Interaction energies of ethane, ethene and ethyne with CuBTC, in kJ/mol, for periodic calculations.

Adsorbate	Approach	E / kJ·mol^{-1}
Ethane	PBE	-7.6
	PBE-D3	-31.6
	M06-L	-24.7
Ethene	PBE	-23.2
	PBE-D3	-48.5
	M06-L	-45.1
Ethyne	PBE	-22.9
	PBE-D3	-40.3
	M06-L	-41.9

Introduction of dispersion corrections to PBE significantly improves the estimates, making them much closer to M06-L than the original PBE values. The main problem with PBE does not therefore seem to be with the fundamental method, but with its incapacity to deal appropriately with dispersive interactions, which the introduction of the DFT-D3 [67] correction seems to deal with rather nicely. Nevertheless, PBE-D3 does seem to lead to somewhat more attractive interaction energies than M06-L and B2PLYP-D.

The two sets of extrapolated values are extremely close. Using a cc-pVDZ- or cc-pVTZ-generated geometry seems to have a negligible effect on the accuracy of the extrapolation. It is also clear that the extrapolation systematically increases the estimated values (i.e., they become less negative). This increase is much more pronounced for cc-pVDZ than cc-pVTZ; *i.e.*, as expected, non-extrapolated estimates of cc-pVTZ are much closer to the extrapolated values than those of cc-pVDZ. In fact, for M06-L and B2PLYP-D, the cc-pVTZ results are so close to the extrapolated results that it becomes questionable whether there is any real advantage in using the extrapolation procedure.

Several groups have obtained isosteric heats of adsorption for C_2H_x in CuBTC, [31, 33, 34, 52, 85, 86] which can be compared against the interaction enthalpies of Table 5. For ethene and ethyne, as the open copper sites should be the first to be filled, the relevant experimental data is found as loading tends to zero. It is very hard to know if the values obtained at moderate loadings are representative of infinite dilution values. Ethane, however, tends not to have a preferential adsorption on the metal centers of MOFs with open metal sites [34, 54, 87, 88], so extrapolation of experimental data to low loadings is perhaps more reliable.

In the case of ethyne adsorbed on CuBTC, Xiang et al. [33] determined an isosteric heat of adsorption of ~44 kJ/mol at ~1 mol/kg. Values at infinite dilution were determined by He et al. [34], 39 kJ/mol, and Cheng and Hu [85], 35.6 kJ/mol, and may be considered more representative. Interestingly, both are lower than the Xiang et al. result for 1 mol/kg loading. Working with other MOFs besides HKUST-1, also containing the open copper sites of a Cu-dimer paddlewheel, several authors obtained results in the 31-35 kJ/mol range at infinite dilution [35, 36, 38, 89], although some discrepant values have also been reported [89]. The M06-L estimates presented in Table 5 fall squarely in the middle of the range of experimental results. Pseudo-B2PLYP-D results lie at the low end of the range and are thus perhaps slightly underestimated, while PBE values are very underestimated, and fail completely to properly describe the heat of adsorption.

In the case of ethene, Heinen et al. [52] have estimated an isosteric heat of adsorption of 33 kJ/mol at ~2 mol/kg of loading, while He et al. [34] have determined a value of 39 kJ/mol at

infinite dilution. These results are, once again, very close to the M06-L and B2PLYP-D-estimated values from Table 5.

In the case of ethane, Wu et al. [86] have estimated an isosteric heat of adsorption of ~25 kJ/mol at ~1 mol/kg of loading. He et al. [34] determined a value of 31 kJ/mol at infinite dilution. Using the "inverse gas chromatography method", Münch and Mertens [31] determined an isosteric heat of adsorption of 29.9 kJ/mol. The three results are 9-17 kJ/mol higher than the extrapolated M06-L and B2PLYP-D values for ethane adsorption, shown in Table 5, much more distant than for ethene and ethyne. This discrepancy would seem to indicate that, unlike for the other adsorbates, the preferential adsorption site for ethane is not the unsaturated metal center. This is in agreement with classical simulations of ethane adsorption in HKUST-1, which show that ethane adsorbs preferentially in the small cages of the framework [90]. It is thus hard to ascertain, based on the limited experimental data available, to which extent M06-L and B2PLYP-D are capable of adequately describing the interaction between the open copper sites and the ethane molecules. It is also important to keep in mind that isosteric heat of adsorption determinations can be tricky, with large ranges in experimentally determined values not being uncommon. For example, in the case of propane in CuBTC, a variation of up to 20 kJ/mol has been reported in different studies[29-31, 91].

For our periodic calculations, PBE-D3 gives an interaction energy estimate for ethane that is 7 kJ/mol more negative than that of M06-L (Table 6). This is a significant difference, and much higher than that observed for ethene and ethyne, in the same table. It is possible that, in the case of ethane, the D3 empirical correction takes into account longer-range attractive interactions (possibly with pore walls) that M06-L does not, thus potentially providing more accurate results.

Other theoretical approaches to modelling the C_2H_x@CuBTC system yield interaction enthalpies similar to the isosteric heats of the experimental benchmarks and to our own calculations. Using the PW91 functional and a periodic model approach, Liu et al.[82] have determined interaction energies of -10.0, -11.4 and -4.4 kJ/mol for C_2H_2, C_2H_4 and C_2H_6, respectively. Given that PW91 is not able to tackle dispersion interactions, these results are very distant from our best results, and are only comparable to our PBE results. Closer, and more realistic results were obtained by Song et al. [83] (-36.9 kJ/mol for C_2H_2) and Campbell et al. [44] (-36.4 kJ/mol for C_2H_4) using the vdW-DF2 functional. Kulkarni and Sholl [51] determined, also with the vdW-DF2 functional, interaction energies of -16.4 and -29.9 kJ/mol for C_2H_6 and C_2H_2, respectively, in CuBTC. These latter values are somewhat underestimated relative to the results from the present study, although it should be noted that they do not result

from an optimization routine, but from a potential energy curve determination for several different C_2H_x-Cu distances. Ji et al. [38], again with the vdW-DF2 functional, obtained adsorption enthalpies for C_2H_2 interacting with the Cu paddlewheel from -30 to -35 kJ/mol, for several MOFs (ex., MOF-505; ZJU-40; several from the NOTT family). This range of calculated adsorption energies is similar to our results incorporating dispersion corrections. Zhang et al. [58], working with C_2H_2 and using the PBE-D2 and PBE functionals, obtained interaction energies of -35.7 and -28.2 kJ/mol, respectively. The first value is very close to our own dispersion-corrected results. You et al. [56] studied C_2H_4 adsorption in the Cu paddlewheel in over 60 MOFs, using PBE-D3 and vdW-DF2. Some of these MOFs possessed paired Cu paddlewheels, thus allowing an adsorbed molecule to interact with two open copper sites at the same time. This led to some exceedingly high values of binding energy being determined, up to -59.7 kJ/mol. Still, most values ranged from -35 to -40 kJ/mol, for PBE-D3, and -30 to -35 kJ/mol for vdW-DF2. In another study by the same group [57], using PBE-D3, 5 different MOFs with open copper sites were tested for the adsorption of C_2H_2, C_2H_4 and C_2H_6, with HKUST-1 binding energy estimates being -34, -40 and -24 kJ/mol, respectively. The other 4 MOFs with open copper sites yielded similar results. These values are somewhat underestimated relative to our own PBE-D3 results. Overall, most results from previous DFT studies on C_2H_x in the Cu_2 paddlewheel are similar to our own. When this does not happen, it is either due to the lack of dispersion interaction correction in the functional used or to not using an optimization routine.

3.4. Topological analysis of the mechanism of adsorption

The Quantum Theory of Molecular Structure [92] has been used extensively to characterize the electronic topology of molecular and supramolecular systems. Herein, we use it to better understand the nature of the Cu-C_2H_x interaction, by using some relevant variables. Among these, $\rho(r)$, electronic energy density, $\nabla^2\rho(r)$, Laplacian of $\rho(r)$, $V(r)$, potential energy density, $G(r)$, kinetic energy density, $H(r)$, total energy density and the electronic localization function (ELF). The values of these variables at bond critical points (bcp) are related to the kind of inter-atomic interaction present [93-103]. Some of the variables are related to each other in useful and revealing ways [98, 99, 101]:

$$H(r) = G(r) + V(r) \tag{2}$$

and

$$\frac{1}{4}\nabla^2\rho(r) = 2\,G(r) + V(r) \tag{3}$$

As G(r) is always positive and V(r) is always negative, $H(r)$ and $\nabla^2\rho$(r) reflect the balance between these two variables.

Several criteria have been proposed to distinguish between open- and closed-shell inter-atomic interactions [93, 94, 96, 99, 101]. In general, open-shell interactions are characterized by high electron density and high potential energy density, and closed-shell interactions by the reverse. A typical covalent bond has $\rho_{bcp} > 0.2\ e\ a_0^{-3}$, $\nabla^2\rho_{bcp} < 0$, $H_{bcp} < 0$ and $G_{bcp}/\rho_{bcp} < 1$. If all of these criteria for a covalent bond are not met, then the interaction can probably be considered open-shell. If some are met but not others, then the interaction has a mixed character.

Table 7. Electron density (ρ, e a0-3), Laplacian of electron density (∇2ρ, e a0-5), total energy density (H (r), Hartrees/e), ratio of kinetic energy density and electron density (G (r) /ρ, Hartrees a03e-2) and electron localization function (ELF), for C_2H_6, C_2H_4 and C_2H_2. Results are for the bond critical points located between the adsorbate and the copper atom in the in-line configurations optimized with the cc-pVTZ basis set.

		ρ	$\nabla^2\rho$	H (r)	G (r) / ρ	ELF
Ethane	PBE	0.0119	0.0369	0.0006	0.7306	0.0400
	M06-L	0.0190	0.0603	-0.0005	0.8203	0.0583
	B2PLYP-D	0.0126	0.0461	0.0007	0.8598	0.0317
Ethene	PBE	0.0288	0.0688	-0.0031	0.7048	0.1277
	M06-L	0.0307	0.0824	-0.0031	0.7744	0.1165
	B2PLYP-D	0.0313	0.0836	-0.0033	0.7745	0.1193
Ethyne	PBE	0.0278	0.0738	-0.0026	0.7573	0.1079
	M06-L	0.0296	0.0889	-0.0025	0.8353	0.0976
	B2PLYP-D	0.0284	0.0856	-0.0023	0.8316	0.0938

The results for the topological characterization of in-line, cc-pVTZ cluster DFT calculations, for all adsorbates and models, are shown in Table 7. The results for cc-pVDZ and for in-line with cc-pVDZ and cc-pVTZ basis sets are shown in Tables S5-S7. A visual representation of the topological analysis, with critical points represented in the molecular structure, is presented in Figure S6. For Table 7, of the parameters presented above, typical of covalent bonds, H_{bcp} and G_{bcp}/ρ_{bcp} are frequently within range, while ρ_{bcp} and $\nabla^2\rho_{bcp}$ are not. That H_{bcp} is negative while $\nabla^2\rho_{bcp}$ is positive shows that (eqs. (2) and (3)) even though the potential energy is higher than the kinetic energy, the difference is not high enough (i.e., the interactions are not strong enough) to generate an electron density maximum in the middle of the bond. Very similar results were obtained for in-between/cc-pVTZ optimizations (Table S6).

Even when $H_{bcp} > 0$, with ethane, it is barely so, indicating a close balance between potential and kinetic energy. H_{bcp} becomes clearly negative for ethene and ethyne, the result of a much stronger interaction, as also indicated by the interaction energies of Table 4. Still, it is worth noticing that even for ethane, where a "pure" London closed-shell interaction was to be expected, some parameters are close to values characteristic of an open-shell interaction. Increasing values of electron density and electron localization function are also a reflection of this fact. Interestingly, $\nabla^2\rho_{bcp}$ does not decrease, as H_{bcp} becomes clearly negative. As per eq. (3), this is an indication that the kinetic energy density also increases for these cases.

Results for cc-pVDZ optimizations show overall similar trends, but with the crucial difference that H_{bcp} is negative far less often. Electron densities are extremely close between cc-pVDZ and cc-pVTZ results, so the H_{bcp} differences are not due to a greater concentration of electrons on the inter-atomic space. This seems to be simply a reflection of a decrease in potential energy density intensity, which would point to a weaker interaction. However, non-extrapolated results from Tables 4 and 5 indicate precisely the opposite – cc-pVDZ predicts stronger interactions than cc-pVTZ, not the reverse.

The results shown in Table 7 for ethene and ethyne closely resemble those typical of open-shell bonds between transition metal atoms. [101] However, in the latter case, $\nabla^2\rho_{bcp}$ values are ~0.001 $e\ a_0^{-5}$, i.e., one order of magnitude smaller than those in Table 7. Similar trends were observed in other cases of transition metal-olefin bond [104]. It is thus perhaps more appropriate to consider the bonds between the open copper sites and the adsorbates as "open shell", in particular in the case of the much more intense π-metal bonds of ethene and ethyne.

4. Conclusions

This work investigated the interaction between C_2H_x molecules and the Cu-dimer paddlewheel. Two sets of DFT calculations were performed, cluster and periodic, yielding consistent results. For cluster calculations, the M06-L and B2PLYP-D functionals seem to describe the interaction similarly, both in terms of geometry and energetics, especially for C_2H_4 and C_2H_2. For periodic calculations, M06-L and PBE-D3 also provided similar results for C_2H_4 and C_2H_2, although PBE-D3 seems to model the C_2H_6 interaction with the paddlewheel better. For cluster calculations, interaction energies for the double-zeta and triple-zeta Dunning basis sets were extrapolated to the complete basis set. Triple-zeta interaction energy results are very close to the extrapolated results, making it questionable whether there is any real advantage in using the extrapolation procedure. For C_2H_2 and C_2H_4, the obtained interaction enthalpies are in good agreement with experimental results and previous DFT studies. C_2H_6 results are less consistent, probably due to stronger competing interactions at other adsorption sites in the experimental measurements. QTAIM-based topological analysis of the optimized clusters confirmed that the π-metal bonds between C_2H_2 and C_2H_4 and the open copper sites of the paddlewheel have an "open shell" character, while for C_2H_6 this is not the case.

Acknowledgements:

This work was developed in the scope of the projects CICECO-Aveiro Institute of Materials POCI-01-0145-FEDER-007679 (Ref. FCT UID/CTM/50011/2019) and Smart Green Homes POCI-01-0247-FEDER-007678, a co-promotion between Bosch Termotecnologia S.A. and the University of Aveiro. These projects are financed by Portugal 2020 under the Competitiveness and Internationalization Operational Program and by the European Regional Development Fund (FEDER).

Associated content

Supporting information (SI) available. The Supporting Information includes a selection of interatomic distances calculated with the cc-pVDZ basis set; representations of the optimized formate clusters at the M06-L/cc-pVTZ and PBE/cc-pVTZ levels of theory; representation of the optimized benzoate cluster at the M06-L/cc-pVDZ level of theory; views of the ethyne and ethane clusters; representations of the QTAIM-based topological analysis; additional results

from the QTAIM-based topological analysis; optimization information for cluster and periodic calculations.

Data availability statement

Additional raw/processed data required to reproduce these findings cannot be shared at this time due to technical or time limitations. They will be made available at the repository of the Stratchclyde University. Information can be requested directly to the corresponding authors of the manuscript.

References

[1] R.B. Eldridge, Ind. Eng. Chem. Res., 32 (1993) 2208-2212.
[2] Y. Wang, S.B. Peh, D. Zhao, Small, 15 (2019) 1900058.
[3] P. Pässler, W. Hefner, K. Buckl, H. Meinass, A. Meiswinkel, H.J. Wernicke, G. Ebersberg, R. Müller, J. Bässler, H. Behringer, D. Mayer, in: Ullmann's Encyclopedia of Industrial Chemistry, Wiley-VCH, 2012, pp. 277-323.
[4] R.T. Yang, Olefin/Paraffin Separations, in: Adsorbents: Fundamentals and Applications, John Wiley & Sons, Inc., Hoboken, New Jersey, 2003, pp. 326-334.
[5] T. Ren, M. Patel, K. Blok, Energy, 31 (2006) 425-451.
[6] B.R. Barnett, M.I. Gonzalez, J.R. Long, Trends Chem., 1 (2019) 159-171.
[7] J. Padin, R.T. Yang, Chem. Eng. Sci., 55 (2000) 2607-2616.
[8] S.U. Rege, R.T. Yang, Chem. Eng. Sci., 57 (2002) 1139-1149.
[9] C.A. Grande, J.D.P. Araújo, S. Cavenati, N. Firpo, E. Basaldella, A.E. Rodrigues, Langmuir, 20 (2004) 5291-5297.
[10] L. Yu, W. Chu, S. Luo, J. Xing, F. Jing, J. Chem. Eng. Data, 62 (2017) 2562-2569.
[11] A.v. Miltenburg, W. Zhu, F. Kapteijn, J.A. Moulijn, Stud. Surf. Sci. Catal., 158 (2005) 979-986.
[12] C. Wu, J. Wang, Y. Fang, Z. Wang, D. Fei, X. Han, Y. Dang, J. Chem. Eng. Data, 64 (2019) 611-618.
[13] J.-R. Li, J. Sculley, H.-C. Zhou, Chem. Rev., 112 (2012) 869-932.
[14] B. Li, H. Wang, B. Chen, Chem. Asian J., 9 (2014) 1474-1498.
[15] Z.R. Herm, E.D. Bloch, J.R. Long, Chem. Mater., 26 (2014) 323-338.
[16] X. Zhao, Y. Wang, D.-S. Li, X. Bu, P. Feng, Adv. Mater., 30 (2018) 1705189.
[17] Z. Zhang, S. Xiang, B. Chen, Cryst. Eng. Commun., 13 (2011) 5983-5992.
[18] Z. Bao, G. Chang, H. Xing, R. Krishna, Q. Rena, B. Chen, Energy Environ. Sci., 9 (2016) 3612-3641.
[19] C. Zhang, L. Wang, G. Maurin, Q. Yang, AIChE J., 64 (2018) 4089-4096.
[20] W.-G. Cui, T.-L. Hu, X.-H. Bu, Adv. Mater., (2019).
[21] E.-Y. Choi, C.A. Wray, C. Hu, W. Choe, Cryst. Eng. Comm., 11 (2009) 553-555.
[22] E.D. Bloch, W.L. Queen, R. Krishna, J.M. Zadrozny, C.M. Brown, J.R. Long, Science, 335 (2012) 1606-1610.
[23] N.A. Khan, S.H. Jhung, J. Hazard. Mater., 325 (2017) 198-213.
[24] Y.-S. Bae, C.Y. Lee, K.C. Kim, O.K. Farha, P. Nickias, J.T. Hupp, S.T. Nguyen, R.Q. Snurr, Angew. Chem. Int. Ed., 51 (2012) 1857-1860.
[25] S. Pu, J. Wang, L. Li, Z. Zhang, Z. Bao, Q. Yang, Y. Yang, H. Xing, Q. Ren, Ind. Eng. Chem. Res., 57 (2018) 1645-1654.
[26] A. Luna-Triguero, J.M. Vicent-Luna, A. Poursaeidesfahani, T.J.H. Vlugt, R. Sánchez-de-Armas, P. Gómez-Álvarez, S. Calero, ACS Appl. Mater. Interfaces, 10 (2018) 16911-16917.
[27] S. Xiang, W. Zhou, Z. Zhang, M.A. Green, Y. Liu, B. Chen, Angew. Chem. Int. Ed., 49 (2010) 4615-4618.
[28] M. Jorge, N. Lamia, A.E. Rodrigues, Colloids and Surfaces A: Physicochemical and Engineering Aspects, 357 (2010) 27-34.
[29] J.W. Yoon, I.T. Jang, K.-Y. Lee, Y.K. Hwang, J.-S. Chang, Bull. Korean Chem. Soc., 31 (2010) 220-223.
[30] M. Rubeš, A.D. Wiersum, P.L. Llewellyn, L. Grajciar, O. Bludsky, P. Nachtigall, J. Phys. Chem. C, 117 (2013) 11159-11167.
[31] A.S. Münch, F.O.R.L. Mertens, Micropor. Mesopor. Mater., 270 (2018) 180-188.
[32] M. Hartmann, S. Kunz, D. Himsl, O. Tangermann, Langmuir, 24 (2008) 8634-8642.

[33] S. Xiang, W. Zhou, J.M. Gallegos, Y. Liu, B. Chen, J. Am. Chem. Soc., 131 (2009) 12415-12419.
[34] Y. He, R. Krishna, B. Chen, Energy Environ. Sci., 5 (2012) 9107-9120.
[35] J. Pang, F. Jiang, M. Wu, C. Liu, K. Su, W. Lu, D. Yuan, M. Hong, Nature Commun., 6 (2015) 7575.
[36] Y. Hu, S. Xiang, W. Zhang, Z. Zhang, L. Wang, J. Bai, B. Chen, Chem. Commun., (2009) 7551-7553.
[37] X. Duan, Q. Zhang, J. Cai, Y. Yang, Y. Cui, Y. He, C. Wu, R. Krishna, B. Chen, G. Qian, J. Mater. Chem. A, 2 (2014) 2628-2633.
[38] F. Chen, D. Bai, D. Jiang, Y. Wang, Y. He, Dalton Trans., 46 (2017) 11469-11478.
[39] Q. Yang, D. Liu, C. Zhong, J.-R. Li, Chem. Rev., 113 (2013) 8261-8323.
[40] F.-X. Coudert, A.H. Fuchs, Coord. Chem. Rev., 307 (2016) 211-236.
[41] M. Fischer, J.R.B. Gomes, M. Fröba, M. Jorge, Langmuir, 28 (2012) 8537-8549.
[42] M. Fischer, J.R.B. Gomes, M. Jorge, Molec. Simul., 40 (2014) 537-556.
[43] C. Campbell, C.A. Ferreiro-Rangel, M. Fischer, J.R.B. Gomes, M. Jorge, J. Phys. Chem. C, 121 (2017) 441-458.
[44] C. Campbell, J.R.B. Gomes, M. Fischer, M. Jorge, J. Phys. Chem. Lett., 9 (2018) 3544-3553.
[45] H.S. Koh, M.K. Rana, A.G. Wong-Foy, D.J. Siegel, J. Phys. Chem. C, 119 (2015) 13451-13458.
[46] T.M. Becker, L.-C. Lin, D. Dubbeldam, T.J.H. Vlugt, J. Phys. Chem. C, 122 (2018) 24488-24498.
[47] M. Fischer, B. Kuchta, L. Firlej, F. Hoffmann, M. Fröba, J. Phys. Chem. C, 114 (2010) 19116-19126.
[48] M. Fischer, F. Hoffmann, M. Fröba, Chem. Phys. Chem., 11 (2010) 2220-2229.
[49] L. Sun, W.-Q. Deng, Wiley Interdiscip. Rev. Comput. Mol. Sci., 7 (2017) e1282.
[50] A.R. Kulkarni, D.S. Sholl, Langmuir, 31 (2015) 8453-8468.
[51] A.R. Kulkarni, D.S. Sholl, J. Phys. Chem. C, 120 (2016) 23044-23054.
[52] J. Heinen, N.C. Burtch, K.S. Walton, C.F. Guerra, D. Dubbeldam, Chem. Eur. J., 22 (2016) 18045-18050.
[53] Y. Ji, L. Ding, Y. Cheng, H. Zhou, S. Yang, F. Li, Y. Li, J. Phys. Chem. C, 121 (2017) 24104-24113.
[54] M. Jorge, M. Fischer, J.R.B. Gomes, C. Siquet, J.C. Santos, A.E. Rodrigues, Ind. Eng. Chem. Res., 53 (2014) 15475-15487.
[55] D. Ongari, D. Tiana, S.J. Stoneburner, L. Gagliardi, B. Smit, J. Phys. Chem. C, 121 (2017) 15135-15144.
[56] W. You, Y. Liu, J.D. Howe, D.S. Sholl, J. Phys. Chem. C, 122 (2018) 8960-8966.
[57] W. You, Y. Liu, J.D. Howe, D. Tang, D.S. Sholl, J. Phys. Chem. C, 122 (2018) 27486-27494.
[58] C. Zhang, Y. Lan, X. Guo, Q. Yang, C. Zhong, AIChE J., 64 (2018) 1389-1398.
[59] A. Castañeda, M. Jurado, O. Matz, M. Calatayud, E. Rojas, A. Maubert, J. Phys.: Conf. Series, 1221 (2019) 012016.
[60] J. Toda, M. Fischer, M. Jorge, J.R.B. Gomes, Chem. Phys. Lett., 587 (2013) 7-13.
[61] S.S.-Y. Chui, S.M.-F. Lo, J.P.H. Charmant, A.G. Orpen, I.D. Williams, Science, 283 (1999) 1148-1150.
[62] C. Prestipino, L. Regli, J.G. Vitillo, F. Bonino, A. Damin, C. Lamberti, A. Zecchina, P.L. Solari, K.O. Kongshaug, S. Bordiga, Chem. Mater., 18 (2006) 1337-1346.
[63] L. Grajciar, P. Nachtigall, O. Bludsky, M. Rubeš, J. Chem. Theory Comput., 11 (2015) 230-238.

[64] J. Hutter, M. Iannuzzi, F. Schiffmann, J. VandeVondele, Wiley Interdiscip. Rev. Comput. Mol. Sci., 4 (2014) 15-25.
[65] J.P. Perdew, K. Burke, M. Ernzerhof, Phys. Rev. Lett., 77 (1996) 3865-3868.
[66] J.P. Perdew, K. Burke, M. Ernzerhof, Phys. Rev. Lett., 78 (1997) 1396.
[67] S. Grimme, J. Antony, S. Ehrlich, H. Krieg, J. Chem. Phys., 132 (2010) 154104.
[68] Y. Zhao, D.G. Truhlar, J. Chem. Phys., 125 (2006) 194101.
[69] S. Goedecker, M. Teter, J. Hutter, Phys. Rev. B, 54 (1996) 1703-17010.
[70] M. Krack, Theor. Chem. Acc., 114 (2005) 145-152.
[71] S.F. Boys, F. Bernardi, Mol. Phys., 19 (1970) 553-566.
[72] M.J. Frisch, G.W. Trucks, H.B. Schlegel, G.E. Scuseria, M.A. Robb, J.R. Cheeseman, G. Scalmani, V. Barone, B. Mennucci, G.A. Petersson, H. Nakatsuji, M. Caricato, X. Li, H.P. Hratchian, A.F. Izmaylov, J. Bloino, G. Zheng, J.L. Sonnenberg, M. Hada, M. Ehara, K. Toyota, R. Fukuda, J. Hasegawa, M. Ishida, T. Nakajima, Y. Honda, O. Kitao, H. Nakai, T. Vreven, J. J. A. Montgomery, J.E. Peralta, F. Ogliaro, M. Bearpark, J.J. Heyd, E. Brothers, K.N. Kudin, V.N. Staroverov, R. Kobayashi, J. Normand, K. Raghavachari, A. Rendell, J.C. Burant, S.S. Iyengar, J. Tomasi, M. Cossi, N. Rega, J.M. Millam, M. Klene, J.E. Knox, J.B. Cross, V. Bakken, C. Adamo, J. Jaramillo, R. Gomperts, R.E. Stratmann, O. Yazyev, A.J. Austin, R. Cammi, C. Pomelli, J.W. Ochterski, R.L. Martin, K. Morokuma, V.G. Zakrzewski, G.A. Voth, P. Salvador, J.J. Dannenberg, S. Dapprich, A.D. Daniels, Ö. Farkas, J.B. Foresman, J.V. Ortiz, J. Cioslowski, D.J. Fox, in, Gaussian, Inc., Wallingford, CT, 2009.
[73] S. Grimme, J. Comput. Chem., 27 (2006) 1787-1799.
[74] T. Schwabe, S. Grimme, Phys. Chem. Chem. Phys., 9 (2007) 3397-3406.
[75] G.D. Purvis, R.J. Bartlett, J. Chem. Phys., 76 (1982) 1910-1918.
[76] T.H. Dunning, J. Chem. Phys., 90 (1989) 1007-1023.
[77] R.A. Kendall, T.H. Dunning, R.J. Harrison, J. Chem. Phys., 96 (1992) 6796-6806.
[78] K.A. Peterson, C. Puzzarini, Theor. Chem. Acc., 114 (2005) 283-296.
[79] D. Figgen, G. Rauhut, M. Dolg, H. Stoll, Chem. Phys., 311 (2005) 227-244.
[80] D.G. Truhlar, Chem. Phys. Lett., 294 (1998) 45-48.
[81] T. Lu, F. Chen, J. Comput. Chem., 33 (2012) 580-592.
[82] K. Liu, D. Ma, B. Li, Y. Li, K. Yao, Z. Zhang, Y. Han, Z. Shi, J. Mater. Chem. A, 2 (2014) 15823-15828.
[83] C. Song, J. Hu, Y. Ling, Y. Feng, D.-L. Chen, Y. He, Dalton Trans., 44 (2015) 14823-14829.
[84] A.K. Wilson, T.v. Mourik, J. Thom H. Dunning, J. Molec. Struct. (Theochem), 388 (1996) 339-349.
[85] P. Cheng, Y.H. Hu, Appl. Surf. Sci., 377 (2016) 349-354.
[86] Y. Wu, Y. Sun, J. Xiao, X. Wang, Z. Li, ACS Sustainable Chem. Eng., 7 (2019) 1557-1563.
[87] J.W. Yoon, J.S. Lee, S. Lee, K.H. Cho, Y.K. Hwang, M. Daturi, C.-H. Jun, R. Krishna, J.-S. Chang, Chem. Eur. J., 21 (2015) 18431-18438.
[88] Z. Bao, S. Alnemrat, L. Yu, I. Vasiliev, Q. Ren, X. Lu, S. Deng, Langmuir, 27 (2011) 13554-13562.
[89] Y. He, B. Li, M. O'Keeffe, B. Chen, Chem. Soc. Rev., 43 (2014) 5618-5656.
[90] E. García-Pérez, J. Gascón, V. Morales-Flórez, J.M. Castillo, F. Kapteijn, S. Calero, Langmuir, 25 (2009) 1725-1731.
[91] M.G. Plaza, A.M. Ribeiro, A. Ferreira, J.C. Santos, U.-H. Lee, J.-S. Chang, J.M. Loureiro, A.E. Rodrigues, Sep. Purif. Technol., 90 (2012) 109-119.
[92] R.F.W. Bader, Chem. Rev., 91 (1991) 893-928.
[93] D. Cremer, E. Kraka, Croat. Chem. Acta, 57 (1984) 1259-1281.
[94] R.F.W. Bader, H. Essén, J. Chem. Phys., 80 (1984) 1943-1960.

[95] A.D. Becke, K.E. Edgecombe, J. Chem. Phys., 92 (1990) 5397-5403.
[96] R.F.W. Bader, in: Atoms in Molecules: A Quantum Theory, Clarenddon Press, Oxford, 1994, pp. 291-292.
[97] E. Espinosa, E. Molins, C. Lecomte, Chem. Phys. Lett., 285 (1998) 170-173.
[98] E. Espinosa, I. Alkorta, I. Rozas, J. Elguero, E. Molins, Chem. Phys. Lett., 336 (2001) 457-461.
[99] P. Macchi, A. Sironi, Coord. Chem. Rev., 238-239 (2003) 383.
[100] B. Silvi, J. Phys. Chem. A, 107 (2003) 3081-3085.
[101] C. Gatti, Z. Kristallogr., 220 (2005) 399-457.
[102] L. Mafra, T. Čendak, S. Schneider, P.V. Wiper, J. Pires, J.R.B. Gomes, M.L. Pinto, J. Am. Chem. Soc., 139 (2017) 389-408.
[103] R. Scatena, Y.T. Guntern, P. Macchi, J. Am. Chem. Soc., 141 (2019) 9382-9390.
[104] A. Sirohiwal, V.R. Hathwar, D. Dey, D. Chopra, Chem. Phys. Chem., 18 (2017) 2859-2863.